

A solvable model for spin polarizations with flow-momentum correspondence

Anum Arslan,^{1,*} Wen-Bo Dong,^{1,†} Guo-Liang Ma,^{2,3,‡} Shi Pu,^{1,§} and Qun Wang^{4,5,¶}

¹*Department of Modern Physics and Anhui Center for fundamental sciences in theoretical physics, University of Science and Tchenology of China, Hefei, Anhui 230026, China*

²*Key Laboratory of Nuclear Physics and Ion-beam Application (MOE), Institute of Modern Physics, Fudan University, Shanghai, 200433, China*

³*Shanghai Research Center for Theoretical Nuclear Physics, NSFC and Fudan University, Shanghai, 200438, China*

⁴*Department of Modern Physics and Anhui Center for Fundamental Sciences in Theoretical Physics, University of Science and Tchenology of China, Hefei, Anhui 230026, China*

⁵*Department of Physics, McGill University, Montreal, Quebec H3A 2T8, Canada*

We present an analytically solvable model based on the blast-wave picture of heavy-ion collisions with flow-momentum correspondence. It can describe the key features of spin polarizations in heavy-ion collisions. With the analytical solution, we can clearly show that the spin polarization with respect to the reaction plane is governed by the directed flow, while the spin polarization along the beam direction is governed by the ellipticity in flow and in transverse emission area. There is a symmetry between the contribution from the vorticity and from the shear stress tensor due to the flow-momentum correspondence. The solution can be improved systematically by perturbation method.

I. INTRODUCTION

In non-central heavy-ion collisions, a large orbital angular momentum of two colliding nuclei can be partially converted into the spin polarization of particles in the final state [1]. This effect is called the global spin polarization [1–5] since it is with respect to the reaction plane formed by the impact parameter and the beam direction which is the same for all particles in one event. In contrast, in hadron-hadron or electron-positron collisions the particle’s spin polarization is with respect to production planes formed by the particle’s momentum and the beam direction which are different for particles with different momenta in one event. The global spin polarization of Λ hyperons was measured by STAR collaboration in Au+Au collisions from 3 to 200 GeV [6–8], by HADES collaboration in Au+Au and Ag+Ag collisions at 2.42-2.55 GeV [9], and by ALICE collaboration in Pb+Pb collisions at 5.02 TeV [10]. The global spin polarization can be described through simulations in hydrodynamic models and transport models such as AMPT and URQMD models [11–19] using Cooper-Frye formula [20, 21]. For recent reviews on global spin polarizations, we refer readers to Refs. [22–30].

It was later proposed in the hydrodynamic model that the spin polarization along the beam direction should behaves as $P^z \sim -\sin(2\phi_p)$ where ϕ_p is the azimuthal angle of the hyperon’s momentum in the transverse plane relative to that of the reaction plane [31]. This prediction was confirmed by the transport model [11]. The SATR collaboration measured P^z but found a sign difference from the theoretical prediction [32], which is called the “sign puzzle”. The first theoretical attempt to explain experimental data was made by the authors of Refs. [33, 34] who found that the temperature vorticity can qualitatively explain the spin polarization along the beam direction. It was later found that a contribution from the shear stress tensor [35–40] can give the correct sign in the longitudinal polarization. It was recently proposed that the projected thermal vorticity and the dissipative correction in a thermal model can describe the behavior of the longitudinal polarization [41]. All these theoretical models show that the global equilibrium has not been reached and off-equilibrium effects have to be considered [42].

Actually the blast wave model was used in Ref. [32] by the STAR collaboration to explain the data for the spin polarization along the beam direction [43, 44]. As is well known, the blast-wave model can describe particle’s momentum spectra on the freeze-out hypersurface [45]. The assumption or picture of the blast wave model is that in high energy heavy-ion collisions the hot and dense matter becomes a thermal source for particle emission. The released particles are assumed to freeze out freely without interacting with other particles. The system is assumed to have

*Electronic address: anumramay@mail.ustc.edu.cn

†Electronic address: wenba@mail.ustc.edu.cn

‡Electronic address: glma@fudan.edu.cn

§Electronic address: shipu@ustc.edu.cn

¶Electronic address: qunwang@ustc.edu.cn

longitudinal boost invariance. The transverse rapidity depends linearly on the freeze-out radius, so the flow velocity is smaller near the center and is larger near the edge of the emission region. In this form, the velocity field looks like a blast wave. Different blast-wave models have been used in describing particle momentum spectra [46–51] and collective flows [52, 53] in heavy-ion collisions at various collision energies.

The spin polarization along the beam direction was explained by the blast-wave picture [54–57] under a naive approximation [32, 43]: $P^z \approx \omega^z/2$. Then it is quite natural to understand the pattern $P^z \sim \sin(2\phi)$ seen in the experiment from the elliptic flow v_2 . As illustrated in Fig. 1, the radial flow velocity in the transverse plane has the form $\mathbf{v} \sim \mathbf{e}_r v_r [1 + v_2 \cos(2\phi)]$, where v_r is the radial flow velocity and $\mathbf{e}_r = (\cos \phi, \sin \phi)$ is the radial direction in the transverse plane. With such a profile of the flow velocity, we immediately obtain $P^z \sim \partial_x v^y - \partial_y v^x \sim (1/r)v_2 v_r \sin(2\phi)$ which is proportional to v_2 . However, the blast-wave model used in Ref. [32, 43] fails to reproduce the global spin polarization because the flow velocity is boost invariant and cannot describe a rotation along y direction. Furthermore, the approximation $P^z \approx \omega^z/2$ is non-relativistic and does not include the relativistic effect which might change the pattern seen in the experiment.

Inspired by the potential of the blast wave picture in describing the spin polarization along the beam direction, we will perform a comprehensive analysis of global and local spin polarization using the modified (or improved) blast wave model (MBWM) [45, 58–61]. The essential part of the MBWM is the profile of the flow velocity u^μ , a four-vector as a function of the space time rapidity η in the longitudinal direction, the transverse rapidity ρ , and the azimuthal angle ϕ_b in the transverse plane. To describe the global spin polarization with respect to the reaction plane, we introduce into the transverse rapidity ρ a term $\alpha_1 \eta \cos \phi_b$ related to the directed flow v_1 , which slightly breaks the boost invariance and leads to a rotation of the system along $-y$ direction. There is also a term $\rho_2 \cos(2\phi_b)$ in ρ related to the elliptic flow v_2 . With this profile of u^μ and under flow-momentum correspondence, we can derive the analytical formula for P^z and P^y as functions of ϕ_p and p_T which capture the key patterns observed in experiments. To our knowledge, this is the first analytically solvable model for spin polarizations in heavy-ion collisions.

In this paper, we adopt the following notations: $g^{\mu\nu} = \text{diag}(1, -1, -1, -1)$ where $\mu, \nu = 0, 1, 2, 3$. Levi-Civita symbol is defined as $\epsilon^{0123} = -\epsilon_{0123} = 1$, $\hbar = k_B = 1$, $x^\mu = (x^0, \mathbf{x})$ and $u \cdot p = u^\mu p_\mu$. The summation of repeated indices is implied if not stated explicitly.

II. DESCRIPTION OF THE MODEL

Our solvable model is based on the modified blast-wave model to which we will give a brief introduction in this section. The overlap region of two colliding nuclei in the transverse plane (xy plane) is shown in Fig. 1 with the nucleus at $x = \pm b/2$ going in the $\pm z$ direction. The perpendicular direction of the reaction plane is then along the y direction.

The QGP can be approximated as a longitudinally boost-invariant system, thus it is natural to use the proper time τ and the space-time rapidity η as variables to replace t and z . Accordingly, the particle's momentum in longitudinal direction can also be described by the transverse mass m_T and the momentum rapidity Y . These variables are defined as

$$\begin{aligned} \tau &= \sqrt{t^2 - z^2}, \quad \eta = \frac{1}{2} \ln \frac{t+z}{t-z}, \\ m_T &= \sqrt{m^2 + p_T^2}, \quad Y = \frac{1}{2} \ln \frac{E_p + p_z}{E_p - p_z}, \end{aligned} \quad (1)$$

where $E_p = \sqrt{|\mathbf{p}|^2 + m^2}$, $\mathbf{p} \equiv (p_x, p_y, p_z)$, and $\mathbf{p}_T = (p_x, p_y)$ with $p_T \equiv |\mathbf{p}_T|$. Therefore the flow four-velocity and the particle's four-momentum can be parameterized as

$$u^\mu(x) = (\cosh \eta \cosh \rho, \sinh \rho \cos \phi_b, \sinh \rho \sin \phi_b, \sinh \eta \cosh \rho), \quad (2)$$

$$p^\mu = (m_T \cosh Y, p_T \cos \phi_p, p_T \sin \phi_p, m_T \sinh Y). \quad (3)$$

Here the transverse expansion of the fireball [45, 55, 57] is described by the transverse rapidity ρ as a function of \tilde{r} (normalized transverse radius), ϕ_b (azimuthal angle of the flow velocity in transverse plane) and η as follows

$$\rho(r, \phi_s, \eta) = \tilde{r} [\rho_0 + \rho_1(\eta) \cos(\phi_b) + \rho_2 \cos(2\phi_b)], \quad (4)$$

where ϕ_b is a function of the azimuthal angle ϕ_s in transverse plane in coordinate space (the function will be defined later), ρ_0 characterizes the mean transverse rapidity of the source element, $\rho_1(\eta) = \alpha_1 \eta$ and ρ_2 describe the azimuthal

anisotropy of the transverse rapidity. In Eq. (4) \tilde{r} is defined as

$$\begin{aligned}\tilde{r} &= \sqrt{\frac{(r \cos \phi_s)^2}{R_x^2} + \frac{(r \sin \phi_s)^2}{R_y^2}} \\ &\approx \frac{r}{R} \left[1 + \frac{1}{2} \epsilon \cos(2\phi_s) \right],\end{aligned}\quad (5)$$

where R_x and R_y are effective radii of the elliptic source in x - and y -direction respectively, and in the second line we have used the approximation $\epsilon \equiv R_y - R_x \ll R \equiv (R_x + R_y)/2$ which works very well in describing data [45]. The functional relation between ϕ_b and ϕ_s is

$$\tan \phi_b = \frac{R_x^2}{R_y^2} \tan \phi_s \approx (1 - 2\epsilon) \tan \phi_s, \quad (6)$$

as shown in Fig. 1. In this paper we will use the ordering of parameters

$$\alpha_1 \sim \rho_2 \sim \epsilon \ll \rho_0. \quad (7)$$

We denote α_1 , ρ_2 and ϵ are $O(\epsilon)$ quantities, while ρ_0 is an $O(1)$ quantity, so α_1 , ρ_2 and ϵ can be treated as perturbations relative to ρ_0 .

The particle's distribution function in phase space $f(x, p)$ is assumed to follow the Boltzmann distribution under the condition $\beta p \cdot u \gg 1$ ($\beta = 1/T$ is the inverse temperature),

$$\begin{aligned}f(x, p) &\equiv f(p \cdot u) = \exp(-\beta p \cdot u) \\ &= \exp \left\{ -\beta [m_T \cosh \rho \cosh(\eta - Y) - p_T \sinh \rho \cos(\phi_b - \phi_p)] \right\},\end{aligned}\quad (8)$$

following Eqs. (2) and (3). One can see that the distribution (8) reaches a maximum when $\eta \approx Y$ and $\phi_b \approx \phi_p$, i.e. the spacetime and momentum rapidities are equal and the flow and momentum azimuthal angles are equal. If we set $\eta = Y$ and $\phi_b = \phi_p$, the distribution reaches a maximum at $p_T/m_T = \tanh \rho$, i.e. the transverse momentum rapidity is equal to the transverse flow rapidity. These conditions are called the flow-momentum correspondence in fireball's expansion.

Physical observables can be computed on the freeze-out hypersurface by

$$\langle O(p) \rangle = \frac{\int d^4x O(x, p) S(x, p)}{\int d^4x S(x, p)}. \quad (9)$$

Here $O(x, p)$ is the physical quantity in phase space corresponding to the observable, and the emission function $S(x, p)$ represents the probability of emitting a particle with the momentum p at the space-time x and thus defines a freeze-out hyper-surface for particle emission at the freeze-out temperature $T = T_f$,

$$S(x, p) = m_T \cosh(\eta - Y) \delta(\tau - \tau_f) \Theta(R - r) f(x, p), \quad (10)$$

where τ_f is the freeze-out proper time and $\Theta(x)$ is the Heaviside step function to require that all particles be emitted within the sphere volume of the radius R . The momentum integrated observables can be obtained by integration over all components of the on-shell momentum

$$\langle O \rangle = \frac{\int d^4x d^3\mathbf{p} E_p^{-1} O(x, p) S(x, p)}{\int d^4x d^3\mathbf{p} E_p^{-1} S(x, p)}. \quad (11)$$

The integral elements of space-time and on-shell momentum are

$$\begin{aligned}d^4x &= \tau r d\tau d\eta dr d\phi_s, \\ \frac{d^3\mathbf{p}}{E_p} &= p_T dp_T dY d\phi_p.\end{aligned}\quad (12)$$

The partially integrated observables can also be obtained by integration over some components of the on-shell momentum. For example, if we look at the p_T and ϕ_p dependence of the observable, we can leave p_T and ϕ_p out of the momentum integral

$$\begin{aligned}\langle O \rangle(p_T) &= \frac{\int d^4x dY d\phi_p O(x, p) S(x, p)}{\int d^4x dY d\phi_p S(x, p)}, \\ \langle O \rangle(\phi_p) &= \frac{\int d^4x dp_T dY p_T O(x, p) S(x, p)}{\int d^4x dp_T dY p_T S(x, p)}.\end{aligned}\quad (13)$$

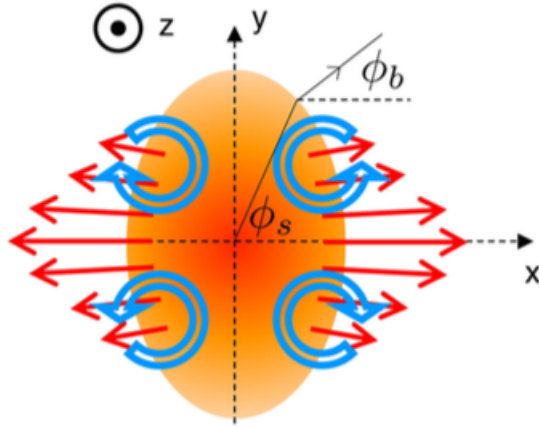


Figure 1: The overlap region of two colliding nuclei. The beam are along $\pm z$ direction. Here the reaction plane is formed by the x and z directions. The figure is taken from Ref. [32]

We will use the above formula to compute the polarization in the global OAM and beam directions as functions of p_T or ϕ_p .

III. COLLECTIVE FLOWS AND SPIN VECTORS: ANALYTICAL RESULTS

With Eqs. (2) and (3) for u^μ and p^μ as well as Eqs. (8) and (10) for $f(p \cdot u)$ and $S(x, p)$, we can calculate the directed flow v_1 as a function of Y and the elliptic flow as a function of p_T as

$$\begin{aligned} v_1(Y) &= \frac{\int d^4x \int dp_T d\phi_p p_T \cos(\phi_p) S(x, p)}{\int d^4x \int dp_T d\phi_p p_T S(x, p)}, \\ v_2(p_T) &= \frac{\int d^4x \int dY d\phi_p \cos(2\phi_p) S(x, p)}{\int d^4x \int dY d\phi_p S(x, p)}. \end{aligned} \quad (14)$$

In the leading order of the flow-momentum correspondence with $\eta = Y$ and $\phi_b = \phi_p$, we can obtain analytical results for $v_1(Y)$ and $v_2(p_T)$ at the central rapidity $Y \approx 0$,

$$\begin{aligned} v_1(Y) &= \alpha_1 Y \frac{\beta}{2R} \frac{N_{v1}}{N_{v0}}, \\ v_2(p_T) &= \left(\rho_2 + \frac{1}{2} \epsilon \rho_0 \right) \frac{\beta}{2R} \frac{N_{v2}(p_T)}{N_{v0}(p_T)} + \epsilon \frac{N_{v2}^\epsilon(p_T)}{N_{v0}(p_T)}, \end{aligned} \quad (15)$$

where we have implied $\beta \equiv 1/T_f$, N_{v0} and N_{v1} are constants in $v_1(Y)$ which are defined through p_T functions $N_{v0}(p_T)$ and $N_{v1}(p_T)$, and $N_{v2}(p_T)$ and $N_{v2}^\epsilon(p_T)$ as well as $N_{v0}(p_T)$ are p_T functions used in $v_2(p_T)$. All these quantities are

defined as

$$\begin{aligned}
N_0 &= \int_0^{p_T^{\max}} dp_T p_T N_0(p_T), \\
N_{v1} &= \int_0^{p_T^{\max}} dp_T p_T N_{v1}(p_T), \\
N_0(p_T) &= \int_0^R dr r m_T K_1(\beta m_T \cosh \bar{\rho}) I_0(\beta p_T \sinh \bar{\rho}), \\
N_{v1}(p_T) &= \int_0^R dr r^2 m_T [m_T \sinh \bar{\rho} K_1'(\beta m_T \cosh \bar{\rho}) I_1(\beta p_T \sinh \bar{\rho}) \\
&\quad + p_T \cosh \bar{\rho} K_1(\beta m_T \cosh \bar{\rho}) I_1'(\beta p_T \sinh \bar{\rho})], \\
N_{v2}(p_T) &= \int_0^R dr r^2 m_T [m_T \sinh \bar{\rho} K_1'(\beta m_T \cosh \bar{\rho}) I_2(\beta p_T \sinh \bar{\rho}) \\
&\quad + p_T \cosh \bar{\rho} K_1(\beta m_T \cosh \bar{\rho}) I_2'(\beta p_T \sinh \bar{\rho})], \\
N_{v2}^\zeta(p_T) &= \int_0^R dr r m_T K_1(\beta m_T \cosh \bar{\rho}) I_2(\beta p_T \sinh \bar{\rho}), \tag{16}
\end{aligned}$$

where $I_{0,1,2}(x)$ and $K_1(x)$ are modified Bessel functions of the first and second kind respectively, $I_{1,2}'(x) = dI_{1,2}(x)/dx$ and $K_1'(x) = dK_1(x)/dx$ are their derivatives, and $\bar{\rho} \equiv (r/R)\rho_0$ is just the ρ_0 part of ρ in (4).

In this paper we aim to calculate the spin polarization of spin-1/2 particles. The spin vectors are defined as

$$\hat{P}_\omega^\mu = -\frac{1}{4m} \epsilon^{\mu\nu\sigma\tau} (1-f) \omega_{\nu\sigma} p_\tau, \tag{17}$$

$$\hat{P}_\xi^\mu = -\frac{1}{2m} \epsilon^{\mu\nu\sigma\tau} (1-f) \frac{p_\tau p^\rho}{E_p} \hat{t}_\nu \xi_{\rho\sigma}, \tag{18}$$

where the vector \hat{t} is given by $\hat{t}^\mu = (1, 0, 0, 0)$ in the laboratory frame, $\omega^{\mu\nu}$ and $\xi^{\mu\nu}$ denote the thermal vorticity and thermal shear stress tensor respectively which are defined as

$$\begin{aligned}
\omega^{\mu\nu} &= -\frac{1}{2} [\partial^\mu (\beta u^\nu) - \partial^\nu (\beta u^\mu)], \\
\xi^{\mu\nu} &= \frac{1}{2} [\partial^\mu (\beta u^\nu) + \partial^\nu (\beta u^\mu)]. \tag{19}
\end{aligned}$$

Note that the polarization vector defined in Eq. (17) is different from Ref. [32], in which \hat{P}_ω^z was assumed to be simply proportional to ω^{xy} .

With Eqs. (2) and (3) for u^μ and p^μ , we can calculate spin vectors \hat{P}_ω^i and \hat{P}_ξ^i (for $i = y, z$) as functions of ϕ_p following Eqs. (17) and (18). In the leading order of the flow-momentum correspondence with $\eta = Y = 0$ and $\phi_b = \phi_p$, the analytical results for \hat{P}_ω^i and \hat{P}_ξ^i can be obtained to $O(\epsilon)$,

$$\begin{aligned}
\hat{P}_\omega^y &\approx \frac{1}{4mT\tau} \left[\alpha_1 \frac{r}{R} (m_T \cosh \rho - p_T \sinh \rho) \cos^2 \phi_p \right. \\
&\quad \left. + C_\omega^\eta(p_T, \phi_p) \partial_{\eta=0} \ln T \right] \\
\hat{P}_\xi^y &\approx \frac{1}{4mT\tau} \frac{p_T}{m_T} \left[\alpha_1 \frac{r}{R} (p_T \cosh \rho - m_T \sinh \rho) \cos^2 \phi_p \right. \\
&\quad \left. + C_\xi^\eta(p_T, \phi_p) \partial_{\eta=0} \ln T \right], \\
\hat{P}_\omega^z &\approx \frac{1}{4mT} \left[2\rho_2 \frac{1}{R} (m_T \cosh \rho - p_T \sinh \rho) \sin(2\phi_p) - \epsilon \frac{1}{r} m_T \sinh \rho \sin(2\phi_p) \right. \\
&\quad \left. + C_\omega^\phi(p_T, \phi_p) \partial_{\phi_s} \ln T + C_\omega^r(p_T, \phi_p) \partial_r \ln T \right], \\
\hat{P}_\xi^z &\approx \frac{1}{4mT} \frac{p_T}{m_T} \left[2\rho_2 \frac{1}{R} (p_T \cosh \rho - m_T \sinh \rho) \sin(2\phi_p) + \epsilon \frac{1}{r} p_T \sinh \rho \sin(2\phi_p) \right. \\
&\quad \left. + C_\xi^\phi(p_T, \phi_p) \partial_{\phi_s} \ln T + C_\xi^r(p_T, \phi_p) \partial_r \ln T \right], \tag{20}
\end{aligned}$$

where C_ω^i and C_ξ^i ($i = \eta, \phi, r$) are coefficients of $\partial_i \ln T$ (temperature gradients) as functions of p_T and ϕ_p , and we have made the approximation $1 - f(p \cdot u) \approx 1$ for under the condition $\beta p \cdot u \gg 1$. We see in Eq. (20) that there are two parts in \hat{P}_ω^i and \hat{P}_ξ^i ($i = y, z$): the kinetic part and temperature gradient part. The latter involves only gradients of T in η, ϕ and r directions and will be vanishing once we take averages of these quantities on the freeze-out hypersurface defined by $\tau = \tau_f$ at $T = T_f$ (the direction of τ is perpendicular to those of ϕ_s and η) as in Eq. (10). So we can safely drop the temperature gradient part.

The analytical expressions in (20) have some good features and symmetries. (a) \hat{P}_ω^y and \hat{P}_ξ^y are proportional to $\cos^2 \phi_p$ and driven by the directed flow v_1 , while \hat{P}_ω^z and \hat{P}_ξ^z are proportional to $\sin(2\phi_p)$ and driven by the elliptic flow v_2 and ellipticity parameter ϵ of the transverse emission region. (b) The coefficients as functions of ρ are different between \hat{P}_ω^i and \hat{P}_ξ^i but closely connected with each other. The collective flow parts of \hat{P}_ω^y and \hat{P}_ω^z (α_1 and ρ_2 terms) are proportional to $m_T \cosh \rho - p_T \sinh \rho$ which is positive definite, while those of \hat{P}_ξ^y and \hat{P}_ξ^z (α_1 and ρ_2 terms respectively) are proportional to $p_T \cosh \rho - m_T \sinh \rho$ which is vanishing when $p_T/m_T = \tanh \rho$, i.e. the transverse momentum rapidity is equal to the transverse flow rapidity, a condition of the flow-momentum correspondence in transverse expansion. So for α_1 and ρ_2 terms, both P^y and P^z are dominated by the kinetic vorticity but not from the shear stress tensor, when the flow-momentum correspondence is implemented. However, in our calculation of the spin polarization, we implement a partial flow-momentum correspondence with $\eta = Y$ and $\phi_b = \phi_p$ but not $p_T/m_T = \tanh \rho$, so the contribution from the shear stress tensor (α_1 and ρ_2 terms) is non-vanishing.

We can insert the quantities in (20) into the second line of (13) to compute the average values P^y and P^z as functions of ϕ_p on the freeze-out hyper-surface defined in Eq. (10),

$$\begin{aligned}
P^y(\phi_p) &= \left\langle \hat{P}_\omega^y + \hat{P}_\xi^y \right\rangle(\phi_p) \\
&\approx \alpha_1 \frac{1}{4mT_f \tau_f R} \frac{1}{N_0} [N_1(2, 1, 2) + N_1(2, 3, 0) - 2N_2(2, 2, 1)] \cos^2 \phi_p, \\
P^z(\phi_p) &= \left\langle \hat{P}_\omega^z + \hat{P}_\xi^z \right\rangle(\phi_p) \\
&\approx \rho_2 \frac{1}{2mT_f R} \frac{1}{N_0} [N_1(1, 1, 2) + N_1(1, 3, 0) - 2N_2(1, 2, 1)] \sin(2\phi_p) \\
&\quad - \epsilon \frac{1}{4mT_f} \frac{1}{N_0} [N_2(0, 1, 2) - N_2(0, 3, 0)] \sin(2\phi_p), \tag{21}
\end{aligned}$$

where the normalization constant N_0 given by the first line of Eq. (16), and $N_{1,2}(n_1, n_2, n_3)$ involve following integrals over p_T and r

$$\begin{aligned}
N_1(n_1, n_2, n_3) &= \int_0^{p_T^{\max}} dp_T \int dr r^{n_1} p_T^{n_2} m_T^{n_3} \cosh \bar{\rho} K_1(\beta m_T \cosh \bar{\rho}) I_0(\beta p_T \sinh \bar{\rho}), \\
N_2(n_1, n_2, n_3) &= \int_0^{p_T^{\max}} dp_T \int dr r^{n_1} p_T^{n_2} m_T^{n_3} \sinh \bar{\rho} K_1(\beta m_T \cosh \bar{\rho}) I_0(\beta p_T \sinh \bar{\rho}). \tag{22}
\end{aligned}$$

In Eq. (22) we have implied $\beta \equiv 1/T_f$. The structure of the collective flow parts (α_1 and ρ_2 terms) of P^y and P^z as functions of ϕ_p is quite similar: (a) P^y is governed by the directed flow v_1 and depends on $\cos^2 \phi_p$, while P^z is governed by the elliptic flow v_2 and depends on $\sin(2\phi_p)$; (b) The prefactors of $\cos^2 \phi_p$ and $\sin(2\phi_p)$ have the same structure except the integrals of P^y have an additional factor r/τ_f in the integrands relative to P^z .

We can also obtain $P^y(p_T)$ and $P_{\sin(2\phi)}^z(p_T)$ by integration over ϕ_p instead of p_T ,

$$\begin{aligned}
P^y(p_T) &= \left\langle \hat{P}_\omega^y + \hat{P}_\xi^y \right\rangle(p_T) \\
&\approx \alpha_1 \frac{1}{8mT_f R \tau_f} \frac{1}{N_0(p_T)} [N_{p1}(2, 0, 2) + N_{p1}(2, 2, 0) - 2N_{p2}(2, 1, 1)], \\
P_{\sin(2\phi)}^z(p_T) &\equiv \left\langle \left(\hat{P}_\omega^z + \hat{P}_\xi^z \right) \sin(2\phi_p) \right\rangle(p_T) \\
&\approx \rho_2 \frac{1}{4mT_f R} \frac{1}{N_0(p_T)} [N_{p1}(1, 0, 2) + N_{p1}(1, 2, 0) - 2N_{p2}(1, 1, 1)] \\
&\quad - \epsilon \frac{1}{8mT_f} \frac{1}{N_0(p_T)} [N_{p2}(0, 0, 2) - N_{p2}(0, 2, 0)], \tag{23}
\end{aligned}$$

centrality	R (fm)	T (MeV)	ρ_0	ρ_2	ϵ	α_1	τ_f (fm/c)
10-20%	11.5	99.5	0.982	0.023	0.05	-0.05	7.8
20-30%	10.3	102	0.937	0.032	0.07	-0.05	6.9
30-40%	9	104	0.894	0.036	0.085	-0.05	5.1
40-50%	7.8	107	0.841	0.052	0.09	-0.05	3.3
50-60%	7	110	0.788	0.058	0.095	-0.05	2.6
60-70%	6.3	116	0.707	0.068	0.11	-0.05	2.3
70-80%	5.5	125	0.608	0.074	0.125	-0.05	2.0

Table I: Parameters in the solvable model that are used in this paper for Au+Au collisions at $\sqrt{s_{NN}} = 200$ GeV.

where $N_0(p_T)$ is given in the fourth line of Eq. (16), and $N_{p1,p2}(n_1, n_2, n_3)$ are integrals over r depending on p_T ,

$$\begin{aligned}
N_{p1}(n_1, n_2, n_3) &= \int dr r^{n_1} p_T^{n_2} m_T^{n_3} \cosh \bar{\rho} K_1(\beta m_T \cosh \bar{\rho}) I_0(\beta p_T \sinh \bar{\rho}), \\
N_{p2}(n_1, n_2, n_3) &= \int dr r^{n_1} p_T^{n_2} m_T^{n_3} \sinh \bar{\rho} K_1(\beta m_T \cosh \bar{\rho}) I_0(\beta p_T \sinh \bar{\rho}).
\end{aligned} \tag{24}$$

In comparison with Eq. (21), the powers of p_T in the integrands of N_{p1} and N_{p2} in Eq. (23) for $P^y(p_T)$ and $P_{\sin(2\phi)}^z(p_T)$ is less than those of N_1 and N_2 for $P^y(\phi_p)$ and $P^z(\phi_p)$ by 1, respectively.

To obtain the centrality dependence of P^y and $P_{\sin(2\phi)}^z$, we need to integrate $N_0(p_T)$ and $N_{p1,p2}(n_1, n_2, n_3)$ over p_T in Eq. (23) as

$$\begin{aligned}
P^y &\approx \alpha_1 \frac{1}{8mT_f R \tau_f} \frac{1}{N_0} [N_1(2, 1, 2) + N_1(2, 3, 0) - 2N_2(2, 2, 1)], \\
P_{\sin(2\phi)}^z &\approx \rho_2 \frac{1}{4mT_f R} \frac{1}{N_0} [N_1(1, 1, 2) + N_1(1, 3, 0) - 2N_2(1, 2, 1)] \\
&\quad - \epsilon \frac{1}{8mT_f} \frac{1}{N_0} [N_2(0, 1, 2) - N_2(0, 3, 0)].
\end{aligned} \tag{25}$$

One can also obtain the above integrated quantities by integration over ϕ_p from Eq. (21). Note that P^y and $P_{\sin(2\phi)}^z$ depend on the centrality through relevant parameters.

IV. COMPARISON WITH DADA

In this section, we will calculate collective flows and spin polarizations using the analytical formula in Sec. III and compare with experimental data.

A. Au+Au collisions at 200 GeV

The parameters that we choose in the solvable model for Au+Au collisions at $\sqrt{s_{NN}} = 200$ GeV and different centralities are listed in Table I. The freeze-out temperature T_f and transverse rapidity parameter ρ_0 are extracted by fitting the transverse momentum spectra [46, 62]. We fit the data for directed flows of $\Lambda/\bar{\Lambda}$ in 10-40% central Au+Au collisions by $\alpha_1 = -0.05$ [63], see Fig. 2. The parameter α_1 is assumed to be independent of the centrality [64]. There is a sizable deviation of the calculated curve for $v_1(Y)$ at larger rapidity from experimental data because of the naive choice of $\rho_1 = \alpha_1 \eta$ and approximations made in Sec. III. Such a deviation can be improved by introducing a cubic term of η into ρ_1 . For elliptic flows, we fit the data for light particles and $\Lambda + \bar{\Lambda}$ in different centralities [62, 65]. As examples, the results for light particles in 30-40% central collisions [62] and $\Lambda + \bar{\Lambda}$ in 10-40% central collisions [65] are shown in Fig. 3, where we see that the fitted curve agrees well with experimental data. From Eq. (15), we can find the parameter dependence of v_2 easily and extract the ρ_2 and ϵ from the elliptic flow.

The spin polarizations P^z and $P_H \equiv -P^y$ can be calculated by Eqs. (21,23). In the calculation we distinguish the contributions from the vorticity and shear stress tensor as in Eq. (20). The experimental data for P^z are available in 20-60% centrality Au+Au collisions at $\sqrt{s_{NN}} = 200$ GeV [32], while the P^y data are available in 20-50% centrality [8].

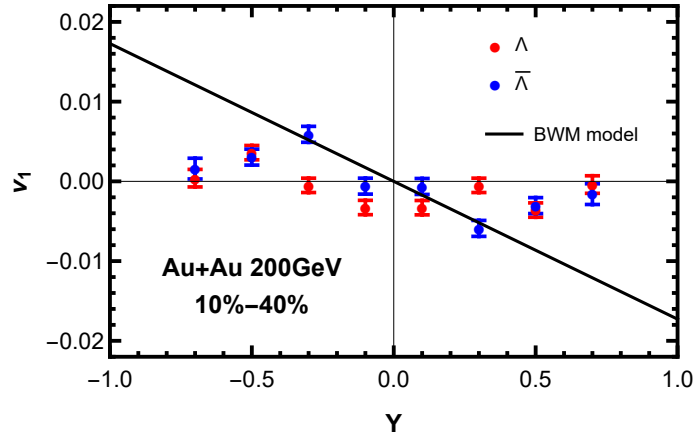


Figure 2: The result for the directed flow v_1 of Λ and $\bar{\Lambda}$ in Au+Au collisions at 200 GeV.

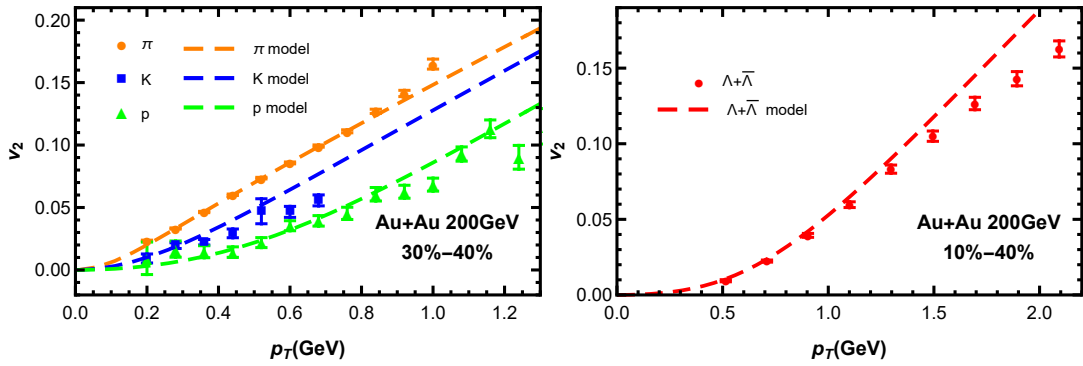


Figure 3: The results for the elliptic flows of light particles (π , K , p) (left panel) and $\Lambda + \bar{\Lambda}$ (right panel) in Au+Au collisions at 200 GeV. The parameters for 20-30% central collisions are chosen to fit $\Lambda + \bar{\Lambda}$ data.

In this paper, the decay parameters of Λ and $\bar{\Lambda}$ are chosen to be $\alpha_\Lambda = -\alpha_{\bar{\Lambda}} = 0.732$. The comparison between the model results and experimental data are shown in Fig. 4. For P^z , the shear contribution is the dominant while the vorticity contribution has an opposite sign relative to the data, consistent with the results by hydrodynamic models [35–37]. This result is different from Ref. [43] because a non-relativistic approximation $P^z \approx \omega^z/2$ is used there. For P_H , we find the vorticity is the dominant source and the shear contribution is negligible, consistent with the previous discussion in Sec. III.

Also we calculated the transverse momentum dependence of polarizations following the analytical formula in Eq.

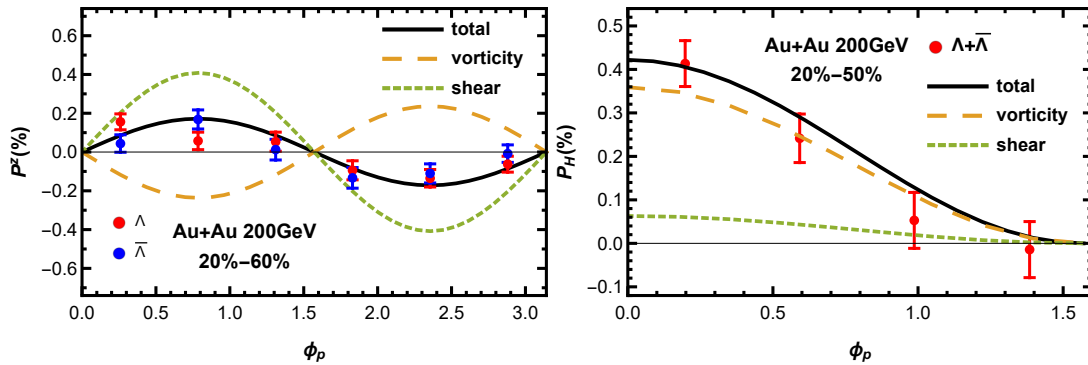


Figure 4: The results for P^z (right panel) and $P_H \equiv -P^y$ (left panel) as functions of ϕ_p following Eq.(21) in Au+Au collisions at 200 GeV. The orange dashed lines and green dotted lines represent the contributions from the vorticity and shear stress tensor, respectively. The black solid lines represent the sums of both contributions.

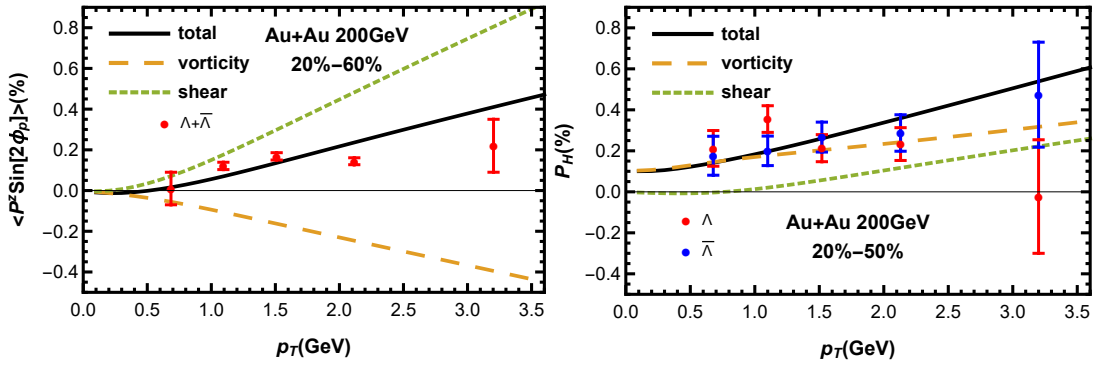


Figure 5: The results for $\langle P^z \sin(2\phi_p) \rangle$ and P_H as functions of p_T in Au+Au collisions at 200 GeV. We use the parameters of 30-40% central collisions as an approximation.

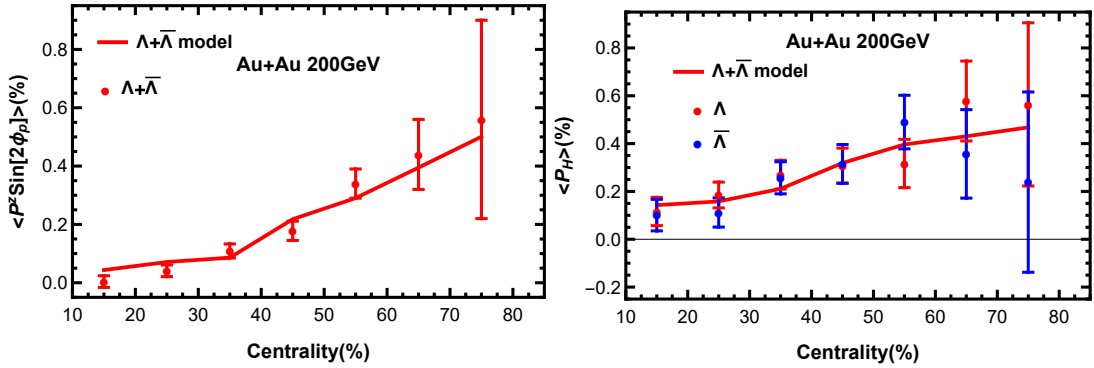


Figure 6: The result for the centrality dependence of P_z and P_H in Au+Au collisions at 200 GeV.

(23). The results are shown in Fig. 5. For $\langle P^z \sin(2\phi_p) \rangle$, the experimental data are almost constant when $p_T \gtrsim 1$ GeV while the calculated result grows with increasing p_T . The vorticity contribution is negative while the shear contribution is positive and has the same sign as the experimental data, consistent with the results by hydrodynamic models. For P_H , the vorticity contribution is dominant at low p_T and increases with growing p_T . The shear contribution is approximately zero at $p_T \lesssim 1$ GeV and increases more rapidly but still smaller than the vorticity contribution.

Using the analytical formula in Eq. (25), we can calculate the centrality dependence of P^z and P_H in the form of $\langle P^z \sin(2\phi_p) \rangle$ and $\langle P_H \rangle$. The comparison of the theoretical result with data is shown in Fig. 6. One can see that the theoretical curve grows from central to peripheral collisions which can describe the experimental data.

centrality	R (fm)	T (MeV)	ρ_0	ρ_2	ϵ	α_1	τ_f (fm/c)
0-10%	13.8	91	1.35	0.016	0.035	-0.002	12.0
10-20%	12.6	94	1.32	0.023	0.051	-0.002	10.1
20-30%	11.5	97	1.28	0.032	0.0695	-0.002	9.0
30-40%	10.0	101	1.23	0.043	0.08	-0.002	6.6
40-50%	8.6	108	1.15	0.048	0.0935	-0.002	4.3
50-60%	7.7	115	1.04	0.052	0.0985	-0.002	3.38
60-70%	7.0	129	0.92	0.056	0.105	-0.002	3.0

Table II: Parameters in the solvable model that are used in this paper for Pb+Pb collisions at $\sqrt{s_{NN}} = 5.02$ TeV.

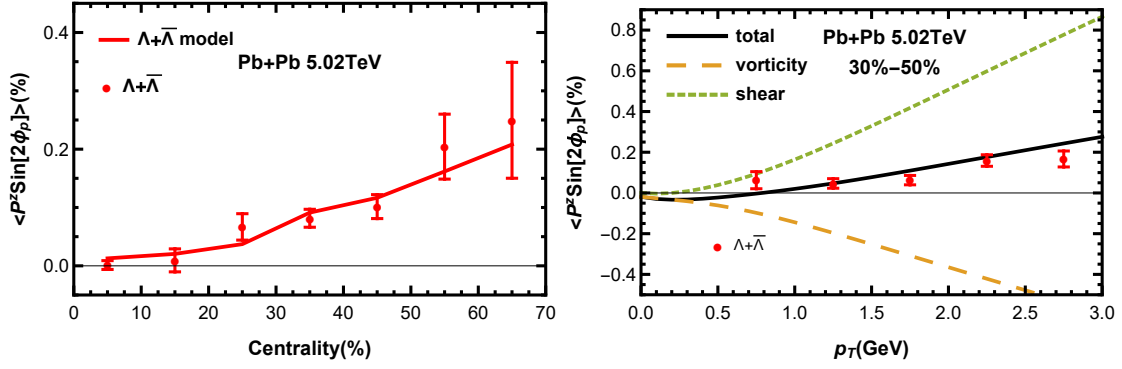


Figure 7: Spin polarizations along the beam direction in Pb+Pb collisions at 5.02 TeV. The parameters for 30-40% central collisions in Table II are used in calculating the transverse momentum dependence of $\langle P^z \sin(2\phi_p) \rangle$.

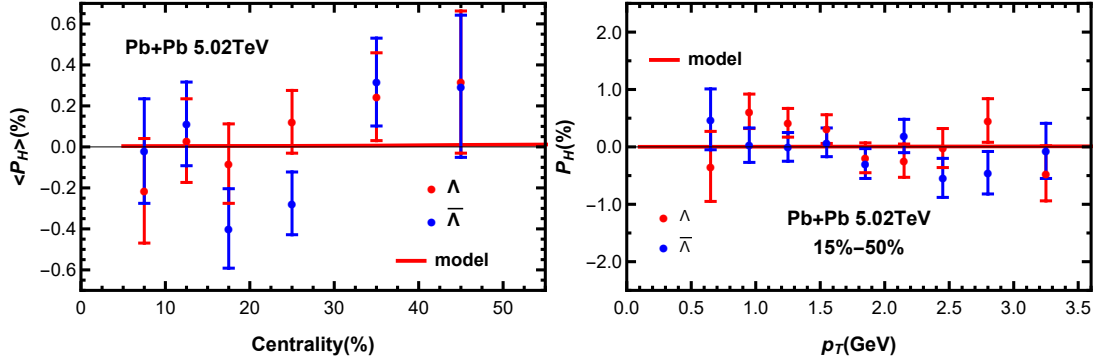


Figure 8: Spin polarizations along the angular momentum direction in Pb+Pb collisions at 5.02 TeV. The parameters for 20-30% central collisions in Table II are used in calculating the transverse momentum dependence of P_H .

B. Pb+Pb collisions at 5.02 TeV

The parameters that we choose in the solvable model for Pb+Pb collisions at $\sqrt{s_{NN}} = 5.02$ TeV and different centralities are listed in Table II. The parameter α_1 is assumed to be independent of the centrality [64]. The freeze-out time is approximated as 1.3 times τ_f at 200 GeV. Other parameters are determined by fitting transverse momentum spectra [66], directed [67] and elliptic flows [68]. The calculated results for the spin polarization variable $\langle P^z \sin(2\phi_p) \rangle$ in the beam direction as functions of centrality and transverse momentum are shown in Fig. 7, which successfully reproduces experimental data [69]. The results for the spin polarization in the angular momentum direction are almost zero as shown in Fig. 8, which is consistent with experimental data [10].

V. SUMMARY

We propose a solvable model for spin polarizations based on the blast-wave picture of heavy-ion collisions with flow-momentum correspondence at the leading order. To our knowledge, this is the first analytically solvable model for spin polarizations in heavy-ion collisions. The analytical solution we find has following features: (1) It not only gives the exact azimuthal angle dependences of spin polarizations in the beam and angular momentum directions, but also gives their exact transverse momentum dependences; (2) It has a symmetry between the contribution from the vorticity and from the shear stress tensor; (3) It can be improved order by order through expansion in $\delta\phi = \phi_b - \phi_p$ and $\delta\eta = \eta - Y$. The solvable model can describe almost all available data for spin polarizations in the beam and angular momentum directions with a few parameters constrained by transverse momentum spectra and collective flows of hadrons.

Acknowledgments

The work was completed during the time when Q.W. visited the nuclear theory group at McGill University as a visiting professor. Q.W. thanks C. Gale and S. Jeon for their hospitality and thanks S. Jeon and X.-Y. Wu for insightful discussions. The work is supported in part by the National Natural Science Foundation of China (NSFC) under Grant Nos. 12135011, 12147101 and 12325507, the Strategic Priority Research Program of the Chinese Academy of Sciences (CAS) under Grant No. XDB34030102, the National Key Research and Development Program of China under Grant No. 2022YFA1604900, and the Guangdong Major Project of Basic and Applied Basic Research under Grant No. 2020B0301030008 (G.-L.M.).

-
- [1] Zuo-Tang Liang and Xin-Nian Wang. Globally polarized quark-gluon plasma in non-central A+A collisions. *Phys. Rev. Lett.*, 94:102301, 2005. [Erratum: *Phys.Rev.Lett.* 96, 039901 (2006)].
 - [2] Sergei A. Voloshin. Polarized secondary particles in unpolarized high energy hadron-hadron collisions? 10 2004.
 - [3] Jian-Hua Gao, Shou-Wan Chen, Wei-tian Deng, Zuo-Tang Liang, Qun Wang, and Xin-Nian Wang. Global quark polarization in non-central A+A collisions. *Phys. Rev. C*, 77:044902, 2008.
 - [4] Barbara Betz, Miklos Gyulassy, and Giorgio Torrieri. Polarization probes of vorticity in heavy ion collisions. *Phys. Rev. C*, 76:044901, 2007.
 - [5] F. Becattini, F. Piccinini, and J. Rizzo. Angular momentum conservation in heavy ion collisions at very high energy. *Phys. Rev. C*, 77:024906, 2008.
 - [6] B. I. Abelev et al. Global polarization measurement in Au+Au collisions. *Phys. Rev. C*, 76:024915, 2007. [Erratum: *Phys.Rev.C* 95, 039906 (2017)].
 - [7] L. Adamczyk et al. Global Λ hyperon polarization in nuclear collisions: evidence for the most vortical fluid. *Nature*, 548:62–65, 2017.
 - [8] Jaroslav Adam et al. Global polarization of Λ hyperons in Au+Au collisions at $\sqrt{s_{NN}} = 200$ GeV. *Phys. Rev. C*, 98:014910, 2018.
 - [9] R. Abou Yassine et al. Measurement of global polarization of Λ hyperons in few-GeV heavy-ion collisions. *Phys. Lett. B*, 835:137506, 2022.
 - [10] Shreyasi Acharya et al. Global polarization of $\Lambda\bar{\Lambda}$ hyperons in Pb-Pb collisions at $\sqrt{s_{NN}} = 2.76$ and 5.02 TeV. *Phys. Rev. C*, 101(4):044611, 2020. [Erratum: *Phys.Rev.C* 105, 029902 (2022)].
 - [11] Xiao-Liang Xia, Hui Li, Ze-Bo Tang, and Qun Wang. Probing vorticity structure in heavy-ion collisions by local Λ polarization. *Phys. Rev. C*, 98:024905, 2018.
 - [12] I. Karpenko and F. Becattini. Study of Λ polarization in relativistic nuclear collisions at $\sqrt{s_{NN}} = 7.7 - 200$ GeV. *Eur. Phys. J. C*, 77(4):213, 2017.
 - [13] Yifeng Sun and Che Ming Ko. Λ hyperon polarization in relativistic heavy ion collisions from a chiral kinetic approach. *Phys. Rev. C*, 96(2):024906, 2017.
 - [14] Hui Li, Long-Gang Pang, Qun Wang, and Xiao-Liang Xia. Global Λ polarization in heavy-ion collisions from a transport model. *Phys. Rev. C*, 96(5):054908, 2017.
 - [15] De-Xian Wei, Wei-Tian Deng, and Xu-Guang Huang. Thermal vorticity and spin polarization in heavy-ion collisions. *Phys. Rev. C*, 99(1):014905, 2019.
 - [16] O. Vitiuk, L. V. Bravina, and E. E. Zabrodin. Is different Λ and $\bar{\Lambda}$ polarization caused by different spatio-temporal freeze-out picture? *Phys. Lett. B*, 803:135298, 2020.
 - [17] Francesco Becattini and Michael A. Lisa. Polarization and Vorticity in the Quark–Gluon Plasma. *Ann. Rev. Nucl. Part. Sci.*, 70:395–423, 2020.
 - [18] Baochi Fu, Kai Xu, Xu-Guang Huang, and Huichao Song. Hydrodynamic study of hyperon spin polarization in relativistic heavy ion collisions. *Phys. Rev. C*, 103(2):024903, 2021.
 - [19] Sangwook Ryu, Vahidin Jupic, and Chun Shen. Probing early-time longitudinal dynamics with the Λ hyperon’s spin polarization in relativistic heavy-ion collisions. *Phys. Rev. C*, 104(5):054908, 2021.
 - [20] F. Becattini, V. Chandra, L. Del Zanna, and E. Grossi. Relativistic distribution function for particles with spin at local thermodynamical equilibrium. *Annals Phys.*, 338:32–49, 2013.
 - [21] Ren-hong Fang, Long-gang Pang, Qun Wang, and Xin-nian Wang. Polarization of massive fermions in a vortical fluid. *Phys. Rev. C*, 94(2):024904, 2016.
 - [22] Qun Wang. Global and local spin polarization in heavy ion collisions: a brief overview. *Nucl. Phys. A*, 967:225–232, 2017.
 - [23] Wojciech Florkowski, Avdhesh Kumar, and Radoslaw Ryblewski. Relativistic hydrodynamics for spin-polarized fluids. *Prog. Part. Nucl. Phys.*, 108:103709, 2019.
 - [24] Xu-Guang Huang, Jinfeng Liao, Qun Wang, and Xiao-Liang Xia. Vorticity and Spin Polarization in Heavy Ion Collisions: Transport Models. *Lect. Notes Phys.*, 987:281–308, 2021.
 - [25] Jian-Hua Gao, Zuo-Tang Liang, Qun Wang, and Xin-Nian Wang. Global Polarization Effect and Spin-Orbit Coupling in Strong Interaction. *Lect. Notes Phys.*, 987:195–246, 2021.
 - [26] Jian-Hua Gao, Guo-Liang Ma, Shi Pu, and Qun Wang. Recent developments in chiral and spin polarization effects in

- heavy-ion collisions. *Nucl. Sci. Tech.*, 31(9):90, 2020.
- [27] Yu-Chen Liu and Xu-Guang Huang. Anomalous chiral transports and spin polarization in heavy-ion collisions. *Nucl. Sci. Tech.*, 31(6):56, 2020.
- [28] Francesco Becattini. Spin and polarization: a new direction in relativistic heavy ion physics. *Rept. Prog. Phys.*, 85(12):122301, 2022.
- [29] Yoshimasa Hidaka, Shi Pu, Qun Wang, and Di-Lun Yang. Foundations and applications of quantum kinetic theory. *Prog. Part. Nucl. Phys.*, 127:103989, 2022.
- [30] Francesco Becattini, Matteo Buzzegoli, Takafumi Niida, Shi Pu, Ai-Hong Tang, and Qun Wang. Spin polarization in relativistic heavy-ion collisions. *Int. J. Mod. Phys. E*, 33(06):2430006, 2024.
- [31] F. Becattini and Iu. Karpenko. Collective Longitudinal Polarization in Relativistic Heavy-Ion Collisions at Very High Energy. *Phys. Rev. Lett.*, 120(1):012302, 2018.
- [32] Jaroslav Adam et al. Polarization of Λ ($\bar{\Lambda}$) hyperons along the beam direction in Au+Au collisions at $\sqrt{s_{NN}} = 200$ GeV. *Phys. Rev. Lett.*, 123(13):132301, 2019.
- [33] Hong-Zhong Wu, Long-Gang Pang, Xu-Guang Huang, and Qun Wang. Local spin polarization in high energy heavy ion collisions. *Phys. Rev. Research.*, 1:033058, 2019.
- [34] Hong-Zhong Wu, Long-Gang Pang, Xu-Guang Huang, and Qun Wang. Local Spin Polarization in 200 GeV Au+Au and 2.76 TeV Pb+Pb Collisions. *Nucl. Phys. A*, 1005:121831, 2021.
- [35] Baochi Fu, Shuai Y. F. Liu, Longgang Pang, Huichao Song, and Yi Yin. Shear-Induced Spin Polarization in Heavy-Ion Collisions. *Phys. Rev. Lett.*, 127(14):142301, 2021.
- [36] F. Becattini, M. Buzzegoli, G. Inghirami, I. Karpenko, and A. Palermo. Local Polarization and Isothermal Local Equilibrium in Relativistic Heavy Ion Collisions. *Phys. Rev. Lett.*, 127(27):272302, 2021.
- [37] Cong Yi, Shi Pu, and Di-Lun Yang. Reexamination of local spin polarization beyond global equilibrium in relativistic heavy ion collisions. *Phys. Rev. C*, 104(6):064901, 2021.
- [38] Wojciech Florkowski, Avdhesh Kumar, Aleksas Mazeliauskas, and Radoslaw Ryblewski. Effect of thermal shear on longitudinal spin polarization in a thermal model. *Phys. Rev. C*, 105(6):064901, 2022.
- [39] David Wagner, Nora Weickgenannt, and Enrico Speranza. Generating tensor polarization from shear stress. *Phys. Rev. Res.*, 5(1):013187, 2023.
- [40] Xiang-Yu Wu, Cong Yi, Guang-You Qin, and Shi Pu. Local and global polarization of Λ hyperons across RHIC-BES energies: The roles of spin hall effect, initial condition, and baryon diffusion. *Phys. Rev. C*, 105(6):064909, 2022.
- [41] Soham Banerjee, Samapan Bhadury, Wojciech Florkowski, Amaresh Jaiswal, and Radoslaw Ryblewski. Longitudinal spin polarization in a thermal model with dissipative corrections. 5 2024.
- [42] Xin-Li Sheng, Nora Weickgenannt, Enrico Speranza, Dirk H. Rischke, and Qun Wang. From Kadanoff-Baym to Boltzmann equations for massive spin-1/2 fermions. *Phys. Rev. D*, 104(1):016029, 2021.
- [43] Sergei A. Voloshin. Vorticity and particle polarization in heavy ion collisions (experimental perspective). *EPJ Web Conf.*, 171:07002, 2018.
- [44] Takafumi Niida. Global and local polarization of Λ hyperons in Au+Au collisions at 200 GeV from STAR. *Nucl. Phys. A*, 982:511–514, 2019.
- [45] Fabrice Retiere and Michael Annan Lisa. Observable implications of geometrical and dynamical aspects of freeze out in heavy ion collisions. *Phys. Rev. C*, 70:044907, 2004.
- [46] B. I. Abelev et al. Systematic Measurements of Identified Particle Spectra in pp , d^+ Au and Au+Au Collisions from STAR. *Phys. Rev. C*, 79:034909, 2009.
- [47] O. Ristea, A. Jipa, C. Ristea, T. Esanu, M. Calin, A. Barzu, A. Scurtu, and I. Abu-Quoad. Study of the freeze-out process in heavy ion collisions at relativistic energies. *J. Phys. Conf. Ser.*, 420:012041, 2013.
- [48] Muhammad Waqas and Bao-Chun Li. Kinetic freeze-out temperature and transverse flow velocity in Au-Au collisions at RHIC-BES energies. *Adv. High Energy Phys.*, 2020:1787183, 2020.
- [49] Jia Chen, Jian Deng, Zebo Tang, Zhangbu Xu, and Li Yi. Nonequilibrium kinetic freeze-out properties in relativistic heavy ion collisions from energies employed at the RHIC beam energy scan to those available at the LHC. *Phys. Rev. C*, 104(3):034901, 2021.
- [50] Dong-Fang Wang, Song Zhang, and Yu-Gang Ma. Nuclear system size scan for freeze-out properties in relativistic heavy-ion collisions by using a multiphase transport model. *Phys. Rev. C*, 101(3):034906, 2020.
- [51] S. Zhang, Y. G. Ma, J. H. Chen, and C. Zhong. Production of Kaon and Λ in Nucleus-Nucleus Collisions at Ultrarelativistic Energy from a Blast-Wave Model. *Adv. High Energy Phys.*, 2015:460590, 2015.
- [52] A. Adare et al. Systematic study of charged-pion and kaon femtoscopia in Au + Au collisions at $\sqrt{s_{NN}}=200$ GeV. *Phys. Rev. C*, 92(3):034914, 2015.
- [53] Yasushi Nara, Asanosuke Jinno, Koichi Murase, and Akira Ohnishi. Directed flow of Λ in high-energy heavy-ion collisions and Λ potential in dense nuclear matter. *Phys. Rev. C*, 106(4):044902, 2022.
- [54] Philip J. Siemens and John O. Rasmussen. Evidence for a blast wave from compress nuclear matter. *Phys. Rev. Lett.*, 42:880–887, 1979.
- [55] Kang Seog Lee, Ulrich W. Heinz, and Ekkard Schnedermann. Search for Collective Transverse Flow Using Particle Transverse Momentum Spectra in Relativistic Heavy Ion Collisions. *Z. Phys. C*, 48:525–541, 1990.
- [56] Ekkard Schnedermann, Josef Sollfrank, and Ulrich W. Heinz. Thermal phenomenology of hadrons from 200-A/GeV S+S collisions. *Phys. Rev. C*, 48:2462–2475, 1993.
- [57] P. Huovinen, P. F. Kolb, Ulrich W. Heinz, P. V. Ruuskanen, and S. A. Voloshin. Radial and elliptic flow at RHIC: Further predictions. *Phys. Lett. B*, 503:58–64, 2001.

- [58] Amaresh Jaiswal and Volker Koch. A viscous blast-wave model for relativistic heavy-ion collisions. 8 2015.
- [59] Z. Yang and Rainer J. Fries. A Blast Wave Model With Viscous Corrections. *J. Phys. Conf. Ser.*, 832(1):012056, 2017.
- [60] Zhidong Yang and Rainer J. Fries. Parameterizing smooth viscous fluid dynamics with a viscous blast wave. *J. Phys. G*, 51(1):015102, 2024.
- [61] Zhidong Yang and Rainer J. Fries. Shear stress tensor and specific shear viscosity of hot hadron gas in nuclear collisions. *Phys. Rev. C*, 105(1):014910, 2022.
- [62] J. Adams et al. Azimuthal anisotropy in Au+Au collisions at $\sqrt{s_{NN}} = 200$ -GeV. *Phys. Rev. C*, 72:014904, 2005.
- [63] Leszek Adamczyk et al. Beam-Energy Dependence of Directed Flow of Λ , $\bar{\Lambda}$, K^\pm , K_s^0 and ϕ in Au+Au Collisions. *Phys. Rev. Lett.*, 120(6):062301, 2018.
- [64] L. Adamczyk et al. Directed Flow of Identified Particles in Au + Au Collisions at $\sqrt{s_{NN}} = 200$ GeV at RHIC. *Phys. Rev. Lett.*, 108:202301, 2012.
- [65] B. I. Abelev et al. Centrality dependence of charged hadron and strange hadron elliptic flow from $\sqrt{s_{NN}} = 200$ -GeV Au + Au collisions. *Phys. Rev. C*, 77:054901, 2008.
- [66] Shreyasi Acharya et al. Production of charged pions, kaons, and (anti-)protons in Pb-Pb and inelastic pp collisions at $\sqrt{s_{NN}} = 5.02$ TeV. *Phys. Rev. C*, 101(4):044907, 2020.
- [67] Shreyasi Acharya et al. Probing the effects of strong electromagnetic fields with charge-dependent directed flow in Pb-Pb collisions at the LHC. *Phys. Rev. Lett.*, 125(2):022301, 2020.
- [68] S. Acharya et al. Anisotropic flow of identified particles in Pb-Pb collisions at $\sqrt{s_{NN}} = 5.02$ TeV. *JHEP*, 09:006, 2018.
- [69] Shreyasi Acharya et al. Polarization of Λ and $\bar{\Lambda}$ Hyperons along the Beam Direction in Pb-Pb Collisions at $\sqrt{s_{NN}} = 5.02$ TeV. *Phys. Rev. Lett.*, 128(17):172005, 2022.